International Journal of Rock Mechanics & Mining Sciences 75 (2015) 196–209

Contents lists available at ScienceDirect

International Journal of Rock Mechanics & Mining Sciences

journal homepage: www.elsevier.com/locate/ijrmms

Automated coal seam detection using a modulated specific energy measure in a monitor-while-drilling context

Raymond Leung *, Steven Scheding [1]

Australian Centre for Field Robotics, Rose Street Building J04, The University of Sydney, NSW 2006, Australia

ARTICLE INFO

Article history:
Received 21 March 2014
Received in revised form
1 October 2014
Accepted 10 October 2014
Available online 21 February 2015

Keywords:
Strata identification
Coal seam detection
Monitor while drilling (MWD)
Drill data feature extraction
Modulated specific energy
Rotation-to-thrust power ratio

ABSTRACT

This paper describes a novel measure called Modulated Specific Energy (SEM) which has been developed for the purpose of characterizing drilled material in open-pit coal mining. In Monitor-While-Drilling (MWD), the information available for coal detection are limited to a small set of drilling parameters that can be measured on a rotary drill rig. Despite this constraint, our analysis shows that MWD can still detect the top of the coal seam consistently without relying on geophysical data — such as bulk density and natural gamma — by using the SEM measure. The proposal utilizes a hypothesized link between a derived drill performance indicator (the rotation-to-thrust power ratio) and geomechanical properties of sedimentary rock strata (shear and compressive strengths) to increase the coal discriminative power of SEM relative to Teale's specific energy measure. Its efficacy is demonstrated using mutual information, a simple threshold strategy and an artificial neural network. The results show the SEM can detect the coal seam interface consistently with a greater margin for error, and overcome the problems of low specificity and high variability observed in existing MWD approaches. By reducing the detection uncertainty, the SEM is able to provide consistent feedback while drilling and eliminate trial-and-error. This makes coal mining processes more integrated and reliable, which in turn improves operational effectiveness and efficiency in coal recovery.

1. Introduction

This paper presents new research and development in real-time strata identification, where in particular, only signals measured on a rotary drill may be exploited and geophysical data are not used. The basic premise is that these measures reflect either directly or indirectly the mechanical responses of the rock to forces imparted by the drill. A specific area of interest is the application of rock mechanics principles and pattern recognition techniques to identify boundaries between coal and non-coal layers in a sedimentary rock mass for open-pit coal mining. An underlying theme is the plausible connection of drill performance indicators with geotechnical parameters such as shearing resistance and compressive strength. This work shows how the Mohr–Coulomb equation inspires the design of a robust feature that is useful for coal seam detection.

It should be noted that successful classification of the major rock layers (such as sandstone, siltstone and coal) depends not only on a strong correlation between these rock types and the drill performance indicators. To achieve consistent results, the devised measures must exhibit a high degree of invariance to changes in operating conditions. Existing Monitor-While-Drilling (MWD) approaches for boundary detection often exploit such correlation [1,2], but they generally exhibit large intra-class variation. For coal seam detectors that rely solely on raw MWD signals such as torque and penetration rate, they are known to be highly sensitive to noise. These attributes (low specificity and high volatility) render them unsuitable for use in the field. Using the same MWD signals, this work demonstrates that it is in fact possible to design a new feature which improves noise tolerance and achieves high specificity in coal seam detection through appropriate signal transformation.

In strip coal mining, a lot of time and energy are devoted to removing the overburden (soil and rock material) that lie above the coal seam. A common method for excavating this waste material in an open-cut coal mine is the *drill-blast cycle*. A key step in this process involves drilling blast holes to a specified depth, then loading them with explosives. Currently, this is mainly a manual-driven process. It involves trial-and-error as operators tend to judge by feel. If the coal seam location is poorly estimated, subsequent detonation will likely cause blast damage and contamination to the coal; both outcomes are counter-productive.

To minimize blast damage, drilling needs to stop at a "stand-off" distance from the top of the coal seam, or at least, before the

* Corresponding author.
E-mail addresses: raymond.leung@sydney.edu.au (R. Leung), steven.scheding@sydney.edu.au (S. Scheding).

[1] Both authors work at the Rio Tinto Centre for Mine Automation which is part of the Australian Centre for Field Robotics (ACFR), School of Aerospace, Mechanical and Mechatronics Engineering at the University of Sydney.

http://dx.doi.org/10.1016/j.ijrmms.2014.10.012

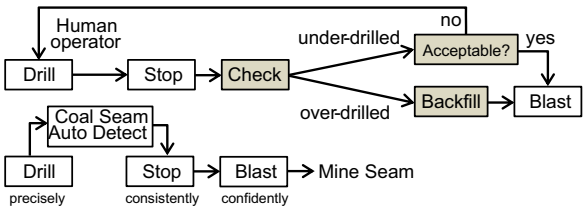

Fig. 1. Main processes in the drill-blast cycle. A contrast between the reactive and proactive approach. (Top) Human operators decide when drilling should stop. Incorrect decisions incur time/energy penalty. (Bottom) Automated coal seam detection via MWD eliminates unnecessary tasks, and streamlines the mining process when done well.

seam is substantially penetrated. The flow chart in Fig. 1 shows that extraneous processes are introduced when mistakes are made. If drilling is stopped too early (a long way above the actual coal seam), then the "resume-drill-stop-check" steps may need to be repeated. If drilling penetrates deep into the seam, the hole may need to be back-filled to insulate the damaging effects of subsequent blasting. These serial dependencies compromise operational effectiveness and mining efficiency.

Automation can increase operational effectiveness and improve coal recovery, by eliminating the unnecessary steps and making processes more reliable. The challenge is to detect the top of the coal seam consistently, using only four mechanical signals provided by the rotary drills currently deployed in the field. These include the penetration rate, rotary speed, weight on bit and torque, which are all monitored while drilling (MWD). This expressly forbids the use of geophysical measurements such as bulk density and natural gamma radiation which are widely regarded as gold standards in coal seam detection.

The objective of automated coal seam detection then is to accurately locate the top of the coal seam — given the MWD constraints — to minimize the amount of debris that ends up in the coal, and volume of coal discarded as waste. This is equivalent to finding the transition from a non-coal rock layer to a coal layer where such an interface exists. With the objective now formally stated, several works will be briefly reviewed to provide an engineering context, explaining how accurate coal seam detection might be achieved. A working hypothesis will be presented in Section 1.2 to relate the proposed features (derived from MWD signals) to material properties of the underlying geology.

1.1. Rock recognition using monitor-while-drilling signals

The works of Teale [3] and Scoble [4,5] are amongst the most influential on this subject. Through empirical analysis, they demonstrated the feasibility of using MWD signals for rock recognition. However, this potential had not been transformed into large scale industrial application to the best of our knowledge. Part of the difficulties may be attributed to low data fidelity, noisy and variable operating conditions. A robust solution that fully integrates with systems in the field has thus far proven elusive. The chief reason, in our view, is that few physical attributes studied-to-date (such as torque, thrust, rotary drilling speed, and penetration rate) possess sufficient discriminative power per se to differentiate coal and non-coal samples on a consistent basis. Although radiometric density measurement can reliably detect coal seams, its operation principle [6] is currently not compatible with monitor-while-drilling.

In the literature, Martin Gonzalez has applied supervised and unsupervised learning techniques such as Back-Propagation Artificial Neural Networks [7,8] and Self Organizing Maps to classify sedimentary rocks [9]. The results pertaining to coal reveal a critical dependence of rock recognition performance on the availability of bulk density (non-MWD) data. Using density, the detection rates (TP and TN) range between 92% and 99%. Without density, false positive and false negative rates (FP and FN) rise to 23.6% (see Tables 6.2 and 7.6 in [9]). Based on these findings, a reasonable conjecture is that deficiencies in the design of coal-sensitive measures in the MWD feature space might be responsible for the performance bottleneck. It is worth noting that neither Martin [9] nor LaBelle [2] proposed any new feature which has been tested on field data.

Feature extraction from rotary drill data has received little attention in the literature. The proposed SEM (Modulated Specific Energy) measure addresses this with a view of improving the robustness of boundary detection via drilling in an MWD context. The SEM exploits two observed properties: (P-1) the mechanical energy required to fracture a rock mass reflects the type of rock being drilled; and (P-2) the rotational power to thrust power ratio (RTPR) has the ability to distinguish coal and non-coal material.

1.2. Geomechanical foundation

The first property (P-1) is exploited using the Specific Energy for Drilling (SED) described in Section 2.1. In [10], Özgen Karacan provided a comprehensive analysis of several mechanical properties of sedimentary rocks using sonic, density and gamma logs, and showed the highest Young's and shear moduli are associated with limestone and competent sandstone layers. When the layer is shale, or coal, these values decrease abruptly. This demonstrates that weaker rock units (such as coal) will be deformed easily when subjected to the high stress and strain conditions that prevail during mining. The findings reinforce Scoble's interpretation in [5] that the SED relates directly to the strength of rocks under a given set of operating conditions. This connection explains one of the motivation for using the SED in our coal seam detection measure.

In rock mechanics, the Mohr–Coulomb criterion provides a basis for understanding rock failure in terms of the rotational and pull-down pressures exerted by the drill

$$\tau_f = b + \tan\phi \cdot \sigma_n \tag{1}$$

Eq. (1) expresses shear stress τ_f as a linear function of the normal compressive stress σ_n. It describes the combined forces required to induce rock breakage. In rotary drilling, when the shearing force is applied parallel to the bedding plane, these material properties (τ_f and σ_n) correspond to the rotational power and thrust power respectively. If the rotation-to-thrust power ratio (RTPR) is able to discern coal and other rock types, then the ratio τ_f/σ_n ought to be different for different rock types. Indeed, several works [11–13] have shown relative differences in shear resistance exist between different sedimentary rocks. Typical values of the internal friction angle ϕ (also known as angle of shear resistance) are shown in Table 1.

As a side note, the values shown in Table 1 are meant to be indicative and not absolute. In practice, τ_f and σ_n both vary depending on porosity, moisture content and other micro-defects, as have been pointed out by Chang [14] and Schöpfer et al. [15]. Interestingly, Poulsen and Adhikary have shown in [16] that despite the wide variation in strength commonly observed in laboratories (see [17]), at large scales, the mass strength of coal is

Table 1
Typical cohesion and friction angle for different rock mass.

Rock type	UCS (MPa)	Cohesion b (MPa)	Friction angle ϕ
Sandstone	37	1.70 ± 0.2	37 ± 2
Siltstone	25	0.55 ± 0.2	25 ± 2
Black Shale	18	0.05 ± 0.04	19 ± 3
Coal	6.5	0.017	16 ± 9

remarkably uniform between coal producing basins and even between continents. At a given mine site, sub-surface local variation might be even less, since the formation process for the sedimentary rock mass should be similar within the same domain. For this work, relative invariance is sufficient. The assumption behind (P-2) is that the shear strength and compressive strength of coal and non-coal rock strata may be inferred from the RTPR. These results render that hypothesis plausible.

1.3. Overview

The remaining paper will demonstrate the effectiveness of the proposed SEM, which combines both the SED and rotation-to-thrust power ratio (RTPR). Section 2 formulates the SEM coal seam detection measure. Section 3 presents the core experimental results: mutual information and a linear classifier are used to assess the utility and detection performance of SEM. Section 4 revisits the problem from the perspective of machine learning and optimization. A neural network implementation is used to validate the SEM approach. Section 5 provides a visual summary, highlighting the differences between the proposed SEM and existing approaches. Discussion and concluding remarks are given in Sections 6 and 7.

2. Formulation

2.1. Specific energy of drilling (SED)

The specific energy of drilling (SED) measures the energy required to fracture rocks. It is defined as the mechanical work done by the drill bit, divided by a unit volume of excavated material [3]. From first principle,

$$\begin{aligned}\mathrm{SED} &= (W_t + W_n)/V \\ &= \langle (F_t, F_n), (v_t, v_n)\delta t\rangle / (\pi r^2 v_n \delta t) \\ &= (\tau\omega + F_n v_n)/(\pi r^2 v_n) \end{aligned} \tag{2}$$

where τ (N m) is the torque, ω (rad s^{-1}) is the rotary speed, F_n (N) is the weight on bit, v_n (m s^{-1}) is the penetration rate, and r (m) is the radius of the rotary drill string. These quantities are depicted in the drill string free body diagram in the inset of Fig. 3.

In the second line, work is related to force via the inner product $W = \langle \mathbf{F}, \mathbf{s}\rangle = \|\mathbf{F}\|\,\|\mathbf{s}\| \cos\theta$. The linear approximation for the displacement, $\mathbf{s} \cong \mathbf{v}\cdot\delta t$ holds when the time element δt is infinitesimally small. In the denominator, the volume is represented by a cylinder with a drill-string radius of r and a height (vertical distance) of $s_n = v_n \delta t$.

In the last line of (2), the denominator represents the volumetric flow rate of the material being excavated. This may be interpreted as the Rate of Excavation (RoE). By convention, v_n is positive when the drill is moving downward, as it fractures rocks and penetrates into new ground. When the drill retracts, it is not doing useful work, so the SED is set to zero for $v_n \le 0$. The numerator in (2) represents mechanical power. Its tangential and normal components are identified in (3):

$$\begin{aligned} P_t &= \tau\omega \;\rightarrow\; \text{Rotational Power} \\ P_n &= F_n v_n \;\rightarrow\; \text{Thrust Power} \end{aligned} \tag{3}$$

Although there exists a strong correlation between a low SED and the presence of coal (this was demonstrated in [5]), using only the SED is insufficient for achieving reliable top of coal seam detection. In Fig. 2, SED can be seen to have low specificity. Normally, a coal band is associated with a trough in the SED signal. However, these troughs can also appear outside the coal band. In particular, two SED false positives are highlighted with concentric circles in Fig. 2.

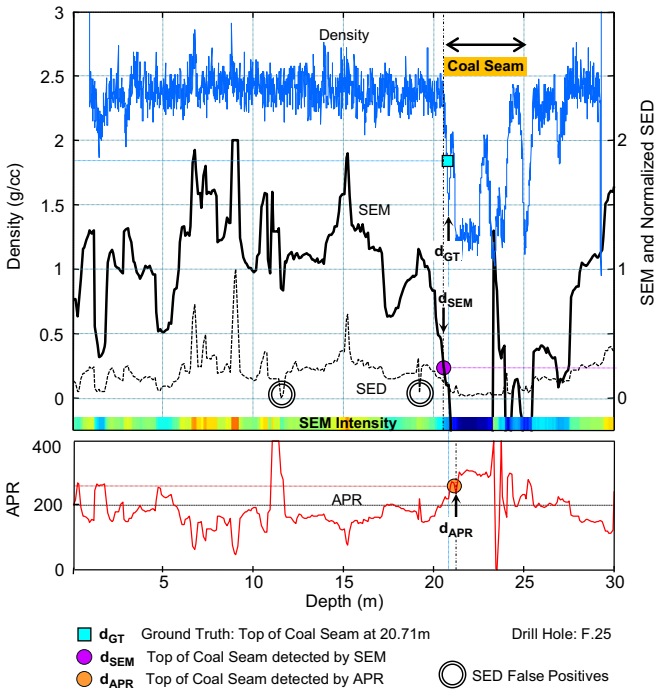

Fig. 2. Pictorial depiction of the SED, SEM and APR. The top of coal location is established by a geophysicist using the measured bulk density.

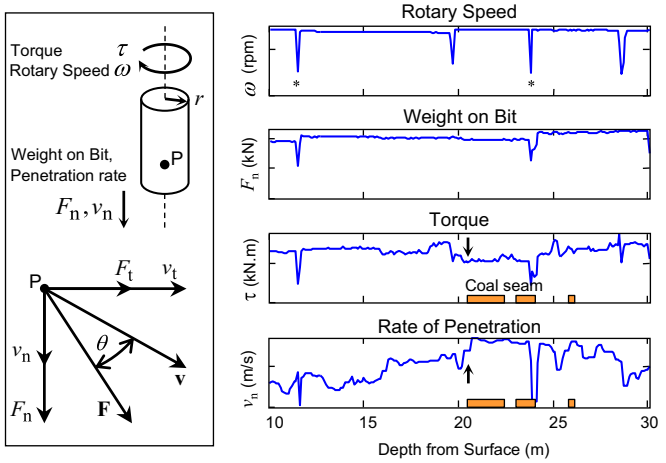

Fig. 3. (Inset) Drill string's free body diagram. (Right) Behavior of MWD signals as drill approaches the coal seam.
Note: *This artifact represents rod change, a normal procedure which extends the reach of the drill. These glitches are filtered out in practice.

2.2. Rotation-to-thrust power ratio (RTPR)

Segui and Higgins have pointed out in [18] both the torque and inverse penetration rate relate to the hardness of rock material. One further observation we make is the penetration rate v_n generally increases and the torque τ simultaneously decreases as a rotary drill enters the coal seam. This behavior, illustrated in Fig. 3, may be modeled by τ/v_n.

Although a diminishing ratio (τ/v_n) captures the right dynamics, numerically, it is sensitive to changes in v_n when $|v_n|$ is small. In practice, this situation arises often in the field, especially when the drill stalls (drill bit is jammed by rock fragments), but also when drilling is interrupted at regular intervals to facilitate "rod change" (to extend the reach of the drill). These events usually generate noise and transients in τ and v_n. Thus, a slight modification is necessary to increase its immunity to noise.

When the hydraulic system is properly regulated, both the weight on bit F_n and rotation speed ω tend to be stable. Thus, $(\tau/v_n)\times(\omega/F_n)$ [which is equivalent to P_t/P_n via (3)] reacts similarly to τ/v_n. The new expression P_t/P_n represents the *rotation-to-thrust power ratio* (RTPR) mentioned in the introduction. To make this more robust, it is normalized to ensure it is bounded. In this paper, the resultant quantity is referred as *rotational work fraction*, and it is defined as

$$\mathrm{RWF}=\frac{W_t}{W_t+W_n}=\frac{P_t}{P_t+P_n}\cdot\frac{\delta t}{\delta t}=\frac{\tau\omega}{\tau\omega+F_n v_n} \tag{4}$$

One remarkable discovery is the tendency of P_t/P_n dropping below a pivot value, as the drill transitions from non-coal material (e.g., mudstone, siltstone, or sandstone) into coal. In this study, the observed rotation-to-thrust power ratio P_t: P_n is approximately 2:1 in the harder material above the coal seam. This ratio shrinks to about 1:1 in the softer material as the drill enters into the coal seam. This means more work is devoted to crushing than shearing the rock. This shift in power balance is depicted in Fig. 4.

The power ratio also has an interesting interpretation. In signal analysis and control systems design, orthogonal projections such as Fourier and Laplace transforms are widely used. From that viewpoint, the components P_t and P_n are analogous to the real and imaginary parts of a phasor $\|\mathbf{p}\|e^{i\psi}$, where $\mathbf{p}=[P_n,P_t]^T$ and $\psi=\tan^{-1}(P_t/P_n)$. It follows the treatment of P_t/P_n is equivalent to studying the phase response. In the area of surface mining and rock recognition using real-time measurements, this perspective provides a way of thinking about the mechanics of rotary drilling, and its connection with the geotechnical properties of a rock mass. It elevates drill energy from a 1D scalar (magnitude only realm) to a 2D vector field (magnitude + phase) even before spatial and temporal variations are considered.

From Fig. 5, two distinct clusters can be seen from the distribution of RWF. This adds credence to the hypothesis that coal and non-coal strata are distinguishable by MWD measures based on differences in shear strength.

Typically, the RWF decreases from 0.70 to about 0.52 as the drill penetrates the coal layer (moving from harder into softer material). Although the specific energy SED in (2) has low specificity, its utility can be boosted by modulating it with a likelihood function. The main reason for combining the SED with RWF is that working in isolation, SED and RWF each has low bias, but high variance. This variance is significantly reduced when both SED and RWF are combined in SEM — this in turn makes the coal seam detector more reliable. The evidence for this will be presented in Section 4.4. Before engaging in detailed analysis, it would be appropriate to complete the description of SEM.

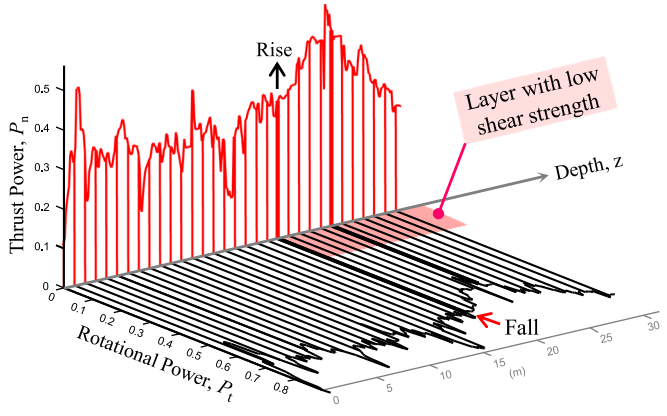

Fig. 4. Shifting power balance between the tangential and normal components illustrated in a 2D vector field. To emphasize the phase relationship, the vectors $\mathbf{p}(z)=[P_n(z),P_t(z)]^T$ are normalized such that $P_n+P_t=1$.

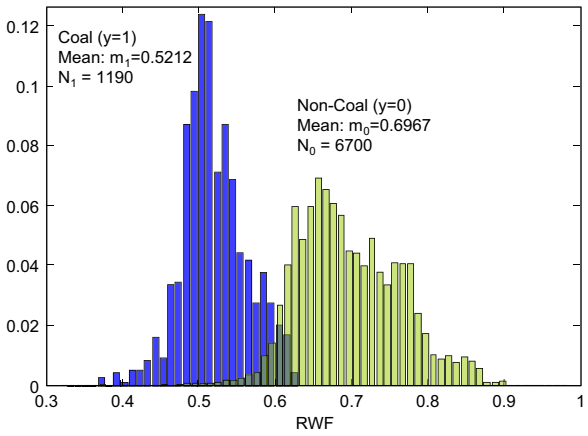

Fig. 5. Bimodal distribution of the RWF.

2.3. Modulated specific energy (SEM)

The proposed SEM is defined as the product of SED and a logistic function of the RWF, denoted $\bar{L}(\cdot)$. Computationally,

$$\begin{aligned}&\mathrm{SEM}=\log_e\left(s\times\bar{L}(w;c,a)\right)+C\\&\text{where } s=\min\{\mathrm{SED}/k_{\mathrm{SED}},e^2\},\quad k_{\mathrm{SED}}=10^8\\&w_n=\alpha\ \mathrm{RWF}_n+(1-\alpha)w_{n-1}\end{aligned} \tag{5}$$

The intermediate variables s and w encode the dependence on SED and RWF, respectively. The expression of s in (5) indicates that the SEM is range limited. Furthermore, exponential filtering is applied to RWF to alleviate noise in the sequence w_n. In this paper, $\alpha=0.5625$ is used throughout. The constant C is set to 2, this changes the interpretation, but not the intrinsic behavior of the SEM. It merely lifts the SEM curve, such that a zero crossing corresponds to the detection of coal. The offset shifts the detection threshold to a more convenient location (0 by default) instead of some arbitrary location like -2 (0.135) in log (linear) scale.

Since the SEM uses an inverted logic (i.e., coal detection occurs closer to 0 than 1), the logistic function in (6) serves as a complementary coal likelihood function:

$$\bar{L}(w;c,a)=\frac{1}{1+\exp(-a(w-c))},\quad a=\frac{\log_e(1-\varepsilon)/\varepsilon}{\min\{c,1-c\}} \tag{6}$$

Fixing ε at 0.01, SEM is left with only one free parameter c which represents the characteristic value of RWF as the drill approaches the coal band. The parameter c specifies the transition point in the logistic function and has a MAP estimated value of $c_0=0.65$ for the data used in this study. The parameter a controls the width of the sigmoid transition. The natural logarithm included in (5) helps amplify weak signals in the proposed SEM. This nonlinearity is advantageous as it sharpens the high-to-low transition at the coal interface — bearing in mind SEM works like an active low logic circuit in top of coal detection.

2.4. Condition adaptive threshold

To increase the resilience of the SEM against changes in operating conditions, it is instructive to consider the impact on the RWF in (4) when the MWD signals are perturbed.

A motivation for doing this is the baseline value $c_0=0.65$ for coal transition in $\bar{L}(w;c_0,a)$ strictly holds only when the rotary drill operates at $\omega_{\max}$ (typically >100 rpm). As the rotation speed drops, $c(\omega)$ declines in a quasi-deterministic manner. As illustrated in Fig. 6, without speed compensation, one consequence of overestimating c [using a baseline value that exceeds the actual value] is the logistic

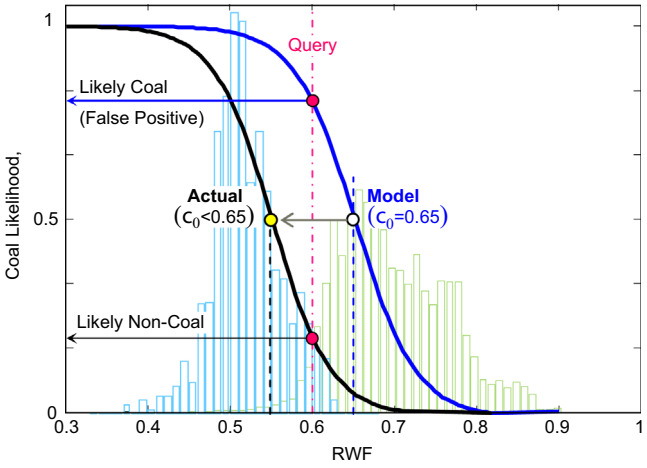

Fig. 6. Shift in likelihood $1-\bar{L}(w;c,a)$ with changing conditions.

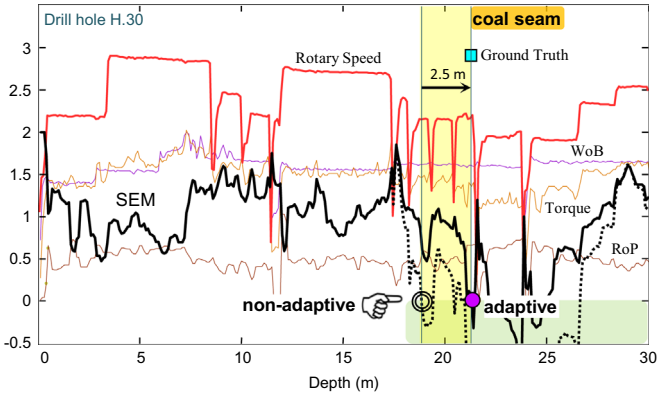

Fig. 7. Improvement from using an adaptive RWF threshold.

Table 2
Experimental evidence that $c(\omega)$ is approximately conditionally independent of $\Delta\tau$, Δv_n and ΔF_n given $\Delta\omega$.

Hole	Relative change (%)				Change factor	Specific value		Prediction error (%)
						Actual	Predict	
	$\Delta\tau$	$\Delta\omega$	ΔF_n	Δv_n	k_ω	c_{actual}	$\hat{c}(\omega)$	Δc
1	−15.4	−44.4	1.5	−14.0	0.556	0.545	0.526	−3.5
2	−17.9	−36.0	−0.9	−18.7	0.640	0.597	0.562	−6.0
3	−12.1	−36.9	5.0	−21.5	0.631	0.561	0.558	−0.6
4	−2.9	−13.1	7.0	−1.9	0.869	0.604	0.635	5.1
5	−11.4	−35.2	7.9	−11.6	0.648	0.537	0.564	5.1
6	−12.8	−30.3	0.2	−9.3	0.697	0.611	0.582	−4.7
7	−13.3	−43.5	8.1	−12.8	0.565	0.503	0.530	5.4
8	−27.3	−64.2	1.2	−12.9	0.358	0.412	0.417	1.2

membership function relaxes its admission requirement, this causes the SEM coal seam detector to return more False Positives (FP).

In general, $\mathrm{RWF}(\tau,\omega,F_n,v_n)$ depends on four variables τ,ω,F_n and v_n. Thus, perturbing these variables in (4),

$$\mathrm{RWF}' = \frac{(\tau+\Delta\tau)(\omega+\Delta\omega)}{(\tau+\Delta\tau)(\omega+\Delta\omega)+(F_n+\Delta F_n)(v_n+\Delta v_n)} = \frac{k_\tau\tau\cdot k_\omega\omega}{k_\tau\tau\cdot k_\omega\omega+k_F F_n\cdot k_v v_n} \quad (7)$$

Through sensitivity analysis, variation in ω was found to have a dominant effect. On average, $\Delta\tau/\tau$ cancels with $\Delta v_n/v_n$, and $\Delta F_n/F_n=\Delta\omega/\omega$. For the purpose of $c(\omega)$ adjustment, Table 2 shows that changes in RWF are approximately conditionally independent of $\Delta\tau$, Δv_n and ΔF_n given $\Delta\omega$. Under this hypothesis ($k_\tau\approx k_v$, $k_F\approx 1$), evaluating RWF′ at $P_t=2P_n$ gives a robust estimate of the coal-specific value

$$\hat{c}(\omega) = \left.\frac{k_\tau\tau\cdot k_\omega\omega}{k_\tau\tau\cdot k_\omega\omega+k_F F_n\cdot k_v v_n}\right|_{k_\tau\approx k_v, k_F=1, \tau\omega=2F_n v_n} = 2k_\omega/(2k_\omega+1) \quad (8)$$

which is stable and dependent only on the scale factor $k_\omega=(\omega_{max}+\Delta\omega)/\omega_{max}\in[0,1]$, where $-\omega_{max}<\Delta\omega\leq 0$. To preserve continuity, $\hat{c}(\omega)$ is multiplied by $\kappa=c_0/(2/3)$ to ensure $c(\omega)=c_0$ when $\Delta\omega=0$ in (8).

Statistically, using $\hat{c}(\omega)$ in place of c_0 reduces the false positive rate from 15% to 4%. Fig. 7 demonstrates one of many instances where a false alarm (incorrect detection) is averted using an adaptive $\hat{c}(\omega)$. As a background note, fluctuation in rotary speed often indicates that the operator is experiencing difficulty drilling the rock mass and is trying different drilling regimes to get back to nominal.

2.5. Adjusted penetration rate (APR)

The adjusted penetration rate is an alternate MWD measure of rock hardness. Defined in (9), it is inversely proportional to the rotation-to-thrust power ratio. One regrettable feature about the APR is that it uses a normalization factor that is strongly data dependent. This generally makes the detector more susceptible to level shifts in the signals.

$$\mathrm{APR}=k_{apr}\times\frac{v_n}{F_n\sqrt{\tau\omega}},\qquad k_{apr}=\mathrm{median}(F_n)\cdot\sqrt{\mathrm{median}(\tau)\times\omega_{max}} \quad (9)$$

In [19], the APR was shown to be effective in differentiating iron ore from shale and BIF (Banded Iron Formation) in a GP (Gaussian Processes) framework [20]. Thus, it would be worthwhile investigating its efficacy for coal seam detection.

3. Experiments

Two experiments were conducted to assess the potential and actual performance of SEM. The first uses mutual information (MI) to assess the utility of different features, viz., how well a sample may be deduced as “coal” or “not coal” using a given measure, such as SED or SEM. The second uses statistical analysis to compare SEM and APR coal seam detection errors on a 35 blast hole drill bench. This bench has referenced geophysics (bulk density) data which serves as the ground truth.

The MWD data was collected from an open-cut coal mine located in Australia, which produces both thermal and semi-soft metallurgical coal [21].

3.1. Mutual information assessment

Mutual information (MI) is defined as $I(X;Y)=H(Y)-H(Y|X)$, where $H(Y)$ represents the entropy of a random process Y associated with the coal label of samples and the conditional entropy $H(Y|X)$ measures the residual uncertainty about Y when the values of some feature X are known [22]. The first experiment uses mutual information to assess the utility of the primary and derived MWD features, viz., how effectively a candidate feature works toward minimizing the uncertainty of the coal labels. Formally, this utility is measured as a reduction in the entropy of Y given X.

The results presented in Table 3 reaffirms the hypothesis that none of the primary MWD signals on their own can effectively

Table 3
Mutual information assessment of feature utility.

X	$I(X;Y)$	X	$I(X;Y)$
Primary MWD Signals		**Derived Features**	
Rotary Speed	0.1548	SED	0.3820
Weight on Bit	0.2586	SEM	**0.5658**
Torque	0.1727	APR	0.5493
Penetration Rate	0.3234	PF*	0.4601
(Torque, Penetration Rate)	0.5255	RWF	0.5350
(Rotary Speed, WoB, Torque, Penetration Rate)	0.5562	**Geophysics**	
		Natural Gamma	0.5452
Spatial		Y	$H(Y)$
Elevation	0.4245	**Entropy**	
(North, East)	0.4036	Coal Label	**0.6006**

PF denotes "power factor". It is defined as $\cos\theta = \langle \mathbf{F}, \mathbf{v} \rangle / \|\mathbf{F}\| \|\mathbf{v}\|$ in (2).

Table 4
APR coal detection rules.

Policy	Requirement
π_A	$[\#(240^+) \geq 7 \mid \Pi_7]$ OR $[\#(310^+) \geq 2 \mid \Pi_5]$ OR $[\#(290^+) \geq 3 \mid \Pi_5$ AND $\#(260^+) \geq 5 \mid \Pi_5]$
π_B	$[\#310^+ \geq 2 \mid \Pi_5]$ OR $[\#290^+ \geq 3 \mid \Pi_5$ AND $\#260^+ \geq 5 \mid \Pi_5]$
π_C	$[\#(310^+) \geq 2 \mid \Pi_5]$
π_D	$[\#(290^+) \geq 1 \mid \Pi_1]$

Table 5
Top of coal seam detection errors.

Detection policy	**Median** (m)	**MAE** (m)	**Mean** (m)	**S.D.** (m)
SEM				
SEM, $T_{\text{sem}} = 0$	0.19	0.34	0.17	0.45
SEM, $T_{\text{sem}} = 0.125$	**0.22**	**0.31**	**0.019**	**0.43**
SEM, $T_{\text{sem}} = 0.25$	0.28	0.39	−0.12	0.51
APR				
APR π_A	**0.28**	**0.37**	**−0.02**	**0.49**
APR π_B	0.46	0.60	0.39	0.64
APR π_C	0.70	0.87	0.69	0.94
APR π_D	0.57	0.57	0.26	0.66

Median= Median Absolute Error, MAE= Mean Absolute Error.

reduce the uncertainty of Y (the coal label) in an information-theoretic sense. However, when one or more variables (especially, the torque and penetration rate) are jointly exploited, they capture about 87.5% (0.5255/0.6006) of the information in Y. A second point to note is the derived MWD features are more effective than the primary MWD signals at capturing information about Y. In particular, for SEM, $I(X;Y)=0.5658$ approaches 94.2% of the entropy bound $H(Y)$. This demonstrates that the SEM has good potential of being an effective coal seam detection measure. Although the natural gamma cannot be used in a MWD context, its MI value (0.5452) has been computed to show that in the absence of geophysics information, the SEM can potentially detect coal just as effectively as measuring natural gamma radiation.

3.2. Coal seam detection performance

The second experiment uses coal seam detection error statistics to contrast the consistency of SEM with its nearest competitor, the APR.

For each drill hole h, the samples $\{s_h(z)\}$ are sorted in order of decreasing elevation z. The features SEM(z) and APR(z) are computed using (5)–(9). For SEM, the top of the coal seam is detected using a simple threshold strategy

$$\hat{z}_{\text{top}} = \max\{z \mid \text{SEM}(z) \leq T_{\text{sem}}\} \tag{10}$$

For APR, a fuzzy set of rules were recommended by the first author of [19]. These detection policies, denoted π, are specified in Table 4, using the short-hand notation $[\#(T_{\text{apr}}^{+}) \geq n \mid \Pi_m]$ which denotes "the number of samples satisfying $\text{APR}(z) \geq T_{\text{apr}}$ in the m-sample neighborhood centered at z must be at least n." The policies π_A to π_D range from prudent to spontaneous. For instance, π_A uses multiple thresholds, and each acceptance criterion (the observation count n) is set inversely proportional to the threshold T_{apr}, to maximize the precision and recall rate.

In Table 5, the error statistics for top of coal seam detection using SEM and APR are reported. These correspond to the stem plot shown in Fig. 8. A negative error indicates coal detection at a shallower depth relative to the ground truth. For SEM, the bias (mean error) is close to zero. Furthermore, SEM is consistent. Its error standard deviation is not very sensitive to changes in the detection threshold.

For the APR, its best performance is comparable to the SEM, but this is achieved using fairly ad hoc and complex detection rules. A major weakness is the APR response must be high enough, and sustained enough, to enable coal seam detection. Although a case can be made to further optimize the APR detection rules, our investigation suggests this is not promising. Significant variation was observed in the signature of APR near the coal seam and its performance did not generalize well to a different test bench. In fact, the movement in error s.d. with respect to detection policies in Table 5 strongly suggests over-fitting.

In Fig. 9, the holes are sorted in order of increasing SEM detection error. The correlation between the error sequences for APR and SEM is $\rho=0.4383$ ($p=0.0084$). This shows the detection errors for APR are weakly correlated with those for SEM, and there is a significant difference in behavior between the two coal seam detection measures, even though their error statistics ($T_{\text{sem}}=0.125$ vs. π_A) are similar on the test sets. In particular, APR detection errors do not increase monotonically with the sorted SEM errors. Large fluctuation in APR errors is observed where the SEM errors are small.

The analysis presented in Section 4 will demonstrate the effectiveness of SEM from a complementary, optimization/machine learning standpoint. An artificial neural network is used to examine the utility of the derived features, to reflect on the optimality of the

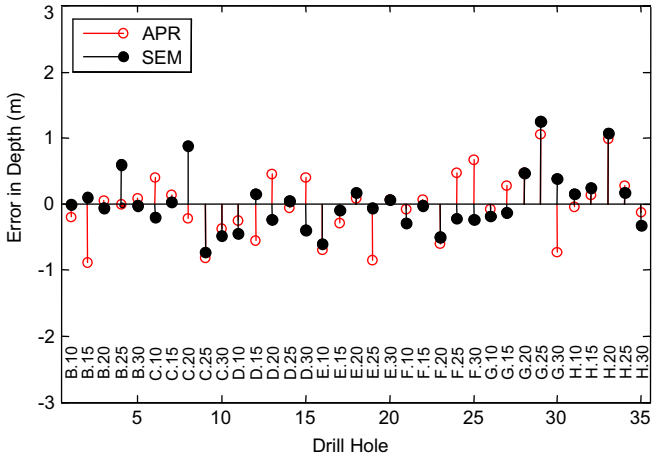

Fig. 8. Top of coal detection errors for SEM ($T_{\text{sem}} = 0.125$) and APR (π_A).

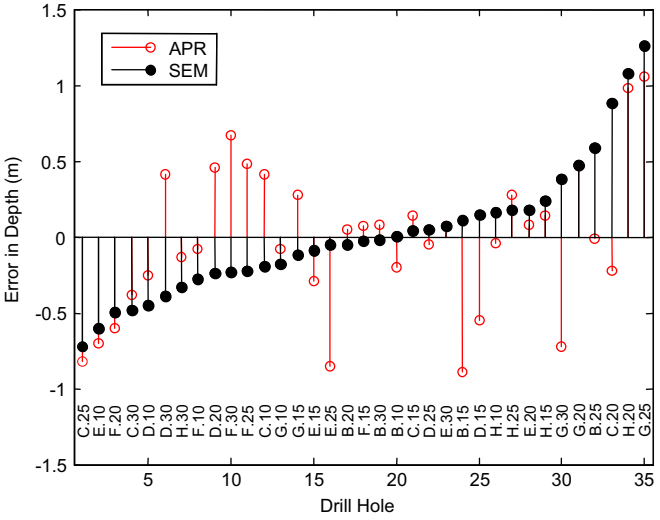

Fig. 9. Coal detection error distribution for SEM and APR.

SEM thresholds, and to test whether non-linear hypotheses lead to improved outcomes.

4. Empirical evaluation using an artificial neural network

The input to the neural network are feature vectors $\mathbf{x} = (x_1, \ldots, x_M)^T$. Each sample $\mathbf{x}^{(n)}$ is associated with a drill hole, this is implicitly encoded in the first three components x_1 to x_3 which represent the spatial coordinates (north, east, elevation). In our model, the NN has m_l sigmoid activation nodes in the hidden layer ($l = 2$). The input and output layers are represented by $l = 1$ and $l = 3$, respectively. In general, there is an $m_{l+1} \times (m_l + 1)$ weights matrix $\Theta^{(l)}$ associated with each layer l. Element $\Theta^{(l)}_{j,k}$ denotes the weight of the connection between node k in layer l and node j in layer $l+1$. Thus, the value of an activation node $a^{(l)}_j$ is computed as

$$a^{(l)}_j = g\left(\sum_{k=0}^{m_l} \Theta^{(l-1)}_{j,k} a^{(l-1)}_k\right) \quad \text{with } a^{(1)}_k = x_k \tag{11}$$

where $g(z) = 1/[1+\exp(-z)]$ and x_0 is set to 1 by convention as a provision for the bias term. For binary classification, the final hypothesis is given by

$$h_\Theta(\mathbf{x}) = a^{(l+1)}_1 |_{\,l=2} = g\left(\sum_{k=0}^{m_2} \Theta^{(2)}_{j,k} a^{(2)}_k\right) \tag{12}$$

$h_\Theta(\mathbf{x}) > 0$ predicts $y = 1$, viz., the sample at location (x_1, x_2, x_3) contains "coal" whereas $h_\Theta(\mathbf{x}) \le 0$ predicts "not coal".

Neural network training seeks to minimize the cost function $J(\Theta)$ in (13). The `fmincg` optimizer [23] was used to solve this via the Polak–Ribière conjugate gradient method:

$$J(\Theta) = \frac{\lambda}{2}\left[\sum_{j=1}^{m_2}\sum_{k=1}^{m_1}\left(\Theta^{(1)}_{j,k}\right)^2 + \sum_{k=1}^{m_2}\left(\Theta^{(2)}_{1,k}\right)^2\right] + \sum_{n=1}^{N}\left[-y^{(n)}\log\left(h_\Theta(\mathbf{x}^{(n)})\right) - (1-y^{(n)})\log\left(1-h_\Theta(\mathbf{x}^{(n)})\right)\right] \tag{13}$$

The first term in $J(\Theta)$ is a regularization expression. The second term is summed over all samples n for a given training set T, where each $\mathbf{x}^{(n)}$ is a feature vector of length $m_1 = M$ at the input layer.

It should be stressed, the decision to use a neural network for analysis does not presuppose that it is the best technique in its class. Its purpose is to provide a common framework for performance evaluation whereby the same detection rules are used irrespective of the chosen features. The neural network is used purely as a vehicle to examine, firstly, the utility of the derived features relative to the primary MWD features such as torque; and secondly, consider the effectiveness and simplicity of using fixed SEM thresholds, as opposed to the cost (and potential benefit) of employing more complex classification techniques.

4.1. Neural network configuration

The neural network structure contained one hidden layer with ten nodes ($m_2 = 10$). The maximum number of iterations allowed during training was limited to 15. The regularization parameter λ in (13) was set to 1, given that all features were normalized as $(X-\mu)/\sigma$.

In subsequent sections, the K-fold cross-validation procedure always divides the data which consists of H holes into two sets for training and testing purpose. For each $k \in \{1, \ldots, K\}$, the training set T_k contains data from $H-(H/K)$ drill holes, and the remaining holes all enter into a complementary test set V_k. However, the sample size N will not be identical for each T_k, as the holes are drilled to slightly different depths. In the experiments, $H = 35$, $K = 5$ and $N \approx 7000$. Each hole $h \in \{1, \ldots, H\}$ must contribute once to one of K test sets. Results were gathered using 32 random initializations of the NN parameters.

4.2. Features utility from a machine learning perspective

Let $w_k[j]$ be a realization of the random variable $W_k = |\Theta^{(1)}_{\cdot,k}|$. Table 6 reports the 95% confidence interval for normalized NN weights, calculated as the expectation of W_k w.r.t. node j in the hidden layer, over all training sets and randomized initialization of the NN parameters. This provides an alternate view of utility in terms of what features a learning algorithm regards as important for minimizing the classification error. The main observations are as follows.

SEM is the most important feature from both the NN and information-theoretic standpoints, in terms of minimizing the classification error and uncertainty. With the exception of the torque, the primary MWD features (rotary speed, weight on bit, and penetration rate) carry much less weight than the derived features (SED, SEM and RWF). These results suggest that the SEM and RWF have greater

influence on coal seam classification performance than the primary MWD signals (features 4–7). This is consistent with the utility predicted by relative mutual information.

4.3. Optimal SEM threshold

In Section 3.2 Table 5, APR performance was shown to be highly sensitive to variation in detection policy. In contrast, SEM has a relatively large region of stability. As a rule of thumb, good coal seam detection performance can be obtained using a static threshold T_{SEM} in the range $[0, 0.25]$. This section contemplates how far this heuristic strays from the optimal point, where the error is minimized by adopting a variable SEM threshold.

The same NN setup is used to facilitate this study. The main step involves looking up the SEM value at the point where the NN first detects the coal seam for each drill hole h, given the samples $\mathbf{x}^{(n)}, n = 1, \ldots, N$ are sorted by holes and processed in order of increasing depth. Using cross-validation, the optimal SEM threshold statistics were computed. The mean and standard deviation, $\mu_{T_{\mathrm{SEM}}}$ and $\sigma_{T_{\mathrm{SEM}}}$, are 0.023 and 0.236 respectively. The results show the fixed SEM thresholds chosen in Table 5 (0 and 0.125) are close to the optimal value (0.023); and the suggested range $R = T_{\mathrm{SEM}}^{\max} - T_{\mathrm{SEM}}^{\min} = 0.25$ is smaller than the variability observed in the SEM threshold when it is allowed to vary (since $R < 2\sigma_{T_{\mathrm{SEM}}}$).

Table 6
Features utility from the classification and information-theoretic viewpoints.

k	Feature, X_k	Normalized NN weights	Normalized mutual information[b]
0	Bias term	0.5131 ± 0.0245	–
1	North	0.4754 ± 0.0120	0.0031
2	East	0.3459 ± 0.0134	0.0028
3	Elevation	**1.2216** ± 0.0309	**0.7068**
4	Rotary Speed	0.3391 ± 0.0129	0.2578
5	Weight on Bit	0.4356 ± 0.0246	0.4305
6	Torque	0.8518 ± 0.0229	0.2875
7	Penetration Rate	0.3449 ± 0.0136	0.5385
8	SED	0.6622 ± 0.0368	0.6360
9	SEM	**1.0000** ± 0.0257	**0.9420**
10	APR	0.7674 ± 0.0148	**0.9145**
11	PF	0.5036 ± 0.0134	0.7661
12	RWF	**1.0369** ± 0.0156	**0.8907**
13	Natural Gamma[a]	1.9949 ± 0.0604	0.9260

[a] Natural gamma radiation cannot be readily measured while drilling.
[b] Defined as $I(X_k; Y)/H(Y)$, $H(Y)$=entropy of coal classification label.

4.4. Statistical analysis and discussion of SEM performance

NN classification and coal seam detection performances are reported in Tables 7 and 8. Specific attention is drawn to the utility of SED, SEM and APR, relative to the primary MWD signals. For SEM, a comparison is made between NN and the simple thresholding approach given in (10).

The distinction between coal detection and classification is as follows. In detection, the NN seeks to find the elevation corresponding to the top of the coal seam. It searches for the point where the NN classifier first emits a 'coal' label ($y = 1$) for a given drill hole. In classification, the NN makes dense predictions. It tests the hypothesis "is this sample coal" repeatedly, on a sequence of feature vectors computed from samples acquired at increasing depth for a given drill hole. The performance metrics for classification are defined below.

Accuracy — In pattern recognition, accuracy is commonly defined as $[n(\text{True Positive}) + n(\text{True Negative})]/n(\text{Total})$, viz., the number of correct detections and omissions, as a percentage of the total number of test samples.

Precision — Precision is defined as $[n(\text{True Positive})]/[n(\text{True Positive}) + n(\text{False Positive})]$, the number of correct detections as a percentage of both correct and incorrect detections.

Recall Rate — Recall is defined as $[n(\text{True Positive})]/[n(\text{True Positive}) + n(\text{False Negative})]$, the number of correct detections as a percentage of the actual number (both hits and misses) that ought to be detected.

For coal and non-coal *classification*, Table 7 shows SEM is more effective than all four primary MWD signals combined. Using ablative analysis, the last three rows suggest the precision and recall rates are mostly influenced by bulk density. Not surprisingly, density is the most preferred type of geophysical data that geophysicists rely upon in determining the ground truth. These results demonstrate two things.

Firstly, using a NN for coal classification, the performance of SEM is superior to APR. SEM has higher precision and recall. It is also competitive with natural gamma.

Secondly, MWD signals are often presumed to be strongly correlated with geophysics density. Whilst this is true to a large extent, the correspondence is not exactly one-to-one. Using SEM, the recall rate for 'coal/non-coal' sample classification peaks around 81%.

This imperfect correspondence may be explained by two observations. First, the average sampling interval of MWD signals is 0.1 m. This represents one tenth the resolution of geophysical data, so it may not be possible to detect finer structures indicated in the ground truth. Second, the mechanical response measured by each MWD signal may exhibit variable time delay — these

Table 7
Coal classification performance using NN.

Augmented features[a]	Accuracy %	Precision %	Recall %
(Rotary Speed, WoB, Torque, Penetration Rate)	91.28 ± 1.51	71.01 ± 6.16	78.25 ± 7.96
APR	91.84 ± 1.36	72.48 ± 5.03	76.49 ± 7.43
SED	90.00 ± 1.17	67.45 ± 4.95	74.17 ± 10.5
SEM	**92.18** $\pm$ **0.87**	**72.62** $\pm$ **2.64**	**81.01** $\pm$ **6.73**
RWF	91.58 ± 0.90	71.07 ± 3.42	79.81 ± 10.5
Natural Gamma[b]	92.35 ± 2.16	72.02 ± 5.64	84.41 ± 8.05
RWF, SEM	92.29 ± 1.16	73.19 ± 3.24	81.36 ± 7.77
RWF, SEM, Gamma[b]	94.05 ± 0.93	78.99 ± 3.75	85.20 ± 5.78
(RWF, SEM, Gamma, Rock Density[b]	99.16 ± 0.02	98.30 ± 1.02	96.42 ± 0.98

[a] In addition to the spatial coordinates (North, East, Elevation).
[b] Natural gamma and long-spaced bulk density are not MWD signals.

Table 8
Neural network top of coal seam detection errors.

Augmented features	Median	MAE	Mean	S.D.(m)
(Rotary Speed, WoB, Torque, Penetration Rate)	0.54	0.99	0.82	1.78
APR	0.42	0.48	0.14	0.58
SED	0.68	0.96	0.09	1.14
SEM	**0.29**	**0.35**	**−0.03**	**0.44**
RWF	0.38	0.59	−0.03	0.94
Natural Gamma	0.15	0.31	−0.02	0.55
RWF, SEM	0.29	0.38	−0.03	0.47
RWF, SEM, Gamma	0.14	0.25	0.02	0.36
(RWF, SEM, Gamma, Rock Density)	0.08	0.23	0.16	0.29

Median = Median Absolute Error, MAE = Mean Absolute Error.

transients are of a physical origin. A manifestation of different time constants may contribute to a loss of synchronicity between the MWD signals.

Although the precision of SEM (72.6%) is rather low, its precision uncertainty ($\pm 2.6\%$) is superior to using raw MWD signals ($\pm 6.1\%$) or natural gamma ($\pm 5.6\%$) with all things being equal. The precision of SEM also needs to be interpreted with care, since most of the sample classification errors actually occur at depths beyond the coal seam. Importantly, top of coal *detection* performance should not be affected by a loss of precision within (or below) the coal seam, since the objective is to prevent drilling through a coal seam during excavation in the first place. The precision and recall rates can certainly be improved by properly excluding samples below the coal seam. However, the true litmus test is whether the first detection error occurs in the interburden (some distance above or below the coal seam). Table 8 shows the magnitude and variability of this error in top of coal detection. This gives better insight into the actual cost of misdetections.

In Table 8, the results demonstrate that high precision top of coal seam detection is possible using SEM. The SEM error is only -0.03 ± 0.44 m. This is as good as the performance achievable with natural gamma, if geophysics (non-MWD) data had been allowed. If instead, primary MWD signals were used, the error would have risen to 0.82 ± 1.78 m. This statistic confirms that using primary MWD signals for coal seam detection is not viable.

Although the SED and RWF each reduces the mean error, they exhibit high variance. Working in synergy, however, the SEM is able to significantly reduce the error s.d. by combining the SED and RWF. Emphatically, the performances for SEM and APR are consistent with (but not better than) those reported in Table 5. This indicates that the SEM coal seam detection performance obtained using a simple adjustable threshold (trivial linear classifier) is nearly optimal without learning a non-linear classifier. The final observation is that fusing SEM with gamma or density can further reduce the error standard deviation (from 0.47 to 0.29 m). This might be useful for constructing a coal-seam surface model. A detailed survey of related topics is beyond the scope of this paper. To investigate further, interested readers are referred to [24,25] on the application of geophysics techniques to coal mining, including the use of seismic reflection and electromagnetic measurements; and [26] on using probabilistic graphical models to learn 3D geological structures from drill data.

5. Visualization

Following the numerical analysis, a visual summary will now be presented to capture the key merits of the SEM approach. Fig. 10 shows a cross-sectional view of the sub-surface modeled using various measures referenced in the main text. The *y*-axis represents the elevation while the *x*-axis is aligned with a row of blast holes. The top two panels (A and B) show the 'Torque/RoP' response and SED, respectively. These represent existing techniques which use raw or energy-based features deriving from MWD data. In panel B, several sedimentary rock types are identified to provide a geological context. Furthermore, the top of coal, top split and bottom of the coal seam are demarcated by lines in white, gray and pink. These lines represent the interpolated ground truth as determined by an experienced geophysicist using the available bulk density data.

5.1. Cross-sectional views

The cross-section images in Fig. 10 show the specificity of each measure to coal. A key observation is the lack of clear definition (blurriness) around the coal seam in panels A and B, which makes these measures unreliable and difficult to use. The middle panels (C and D) show that the RWF response is far more selective to the coal band. This clear separation (sharp transition from light to dark blue at around 10 m) makes SEM an excellent candidate for coal interface detection as it has high specificity. The bottom panels (E and F) show the results which would have been obtained if natural gamma and bulk density (non-MWD, geophysical data) had been used.

5.2. Cumulative distribution of the error

Collectively, the coal seam detection errors for all 35 holes in the bench — from which the statistics in Table 8 were based — are shown in Fig. 11. To facilitate a worst case analysis, these results are converted into a cumulative error distribution, which is displayed in Fig. 12. Looking at the errors at the 5th and 95th percentile, the strength of the SEM becomes apparent.

SEM has a coal seam detection error bounded by -1.18 m and 0.973 m. Its performance curve is closest to the geophysics benchmark, viz., the curve corresponding to bulk density (tightly clustered around 0). Although APR has similar average performance as SEM, its error already exceeds 2 m at the 90th percentile band, thus its error is practically not upper-bounded. The worst performances are associated with *existing* MWD measures, such as Torque and RoP, which for 30% of the holes, they exhibit an error of 1 m or more.

The results thus far have demonstrated the superior performance of SEM relative to other measures without explaining why it is. To appreciate how these differences arise, the responses of MWD measures will now be examined at the critical junction where the non-coal to coal transition takes place. The overarching objective is to highlight the behavior of MWD signals as drilling moves across lithological boundaries, to fully appreciate the reliability and localization properties of various MWD measures.

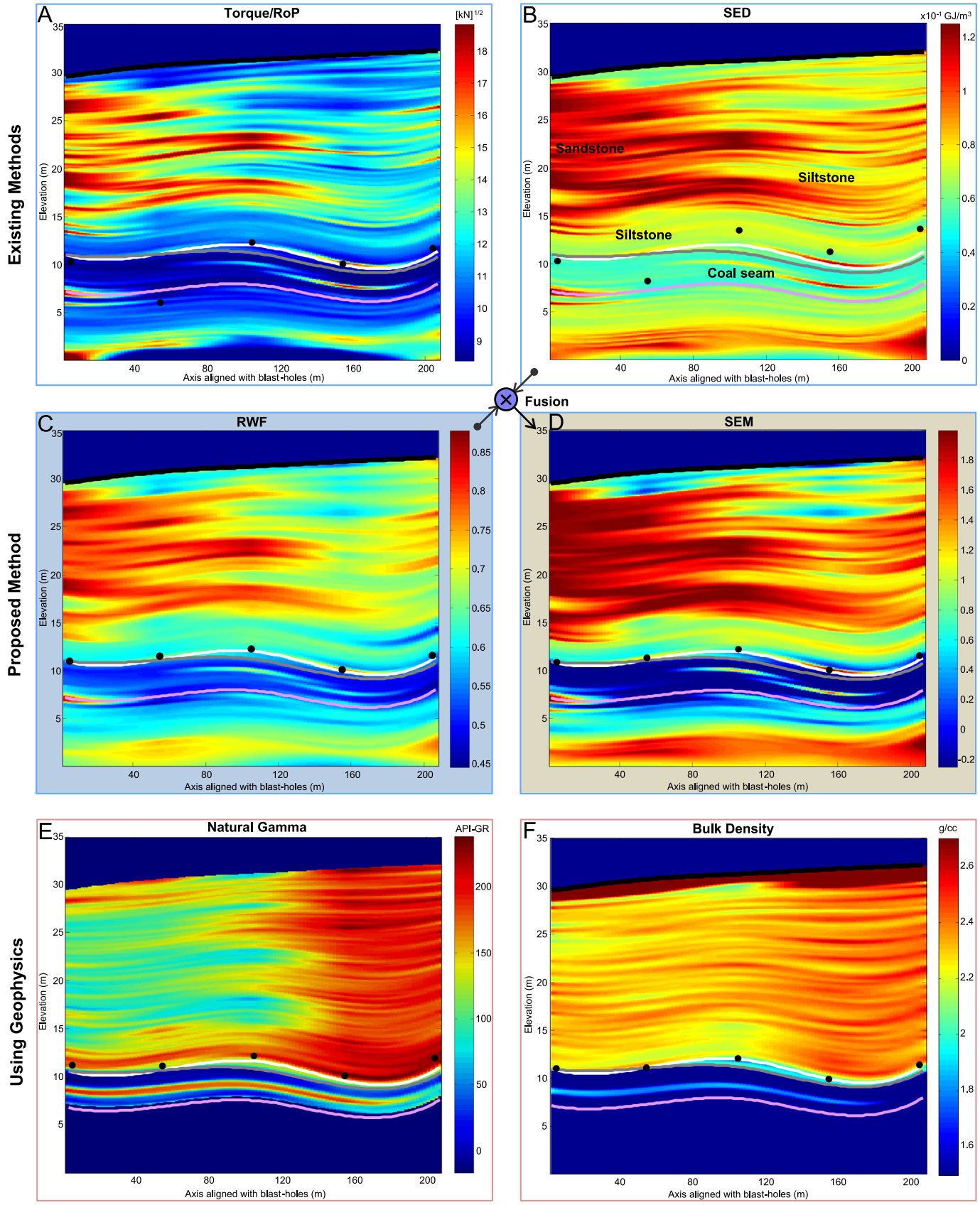

Fig. 10. Cross-sectional view of the sub-surface based on various measures. Top: Existing methods (A) Torque/RoP, (B) SED. Middle: Proposed methods (C) RWF, (D) SEM. Bottom: Geophysics reference (E) Natural Gamma, (F) Bulk Density. Black dots show the coal seam position estimated by the neural network (for 5 blast holes) using the designated measure. The white line marks the ground truth for the top of coal. (For interpretation of the references to color in this figure, the reader is referred to the web version of this paper.)

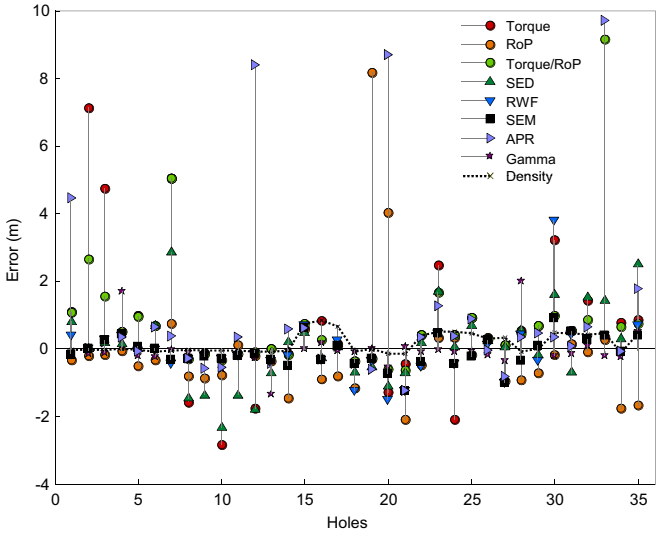

Fig. 11. Coal seam detection error for various measures across the entire bench. Detections made by neural network.

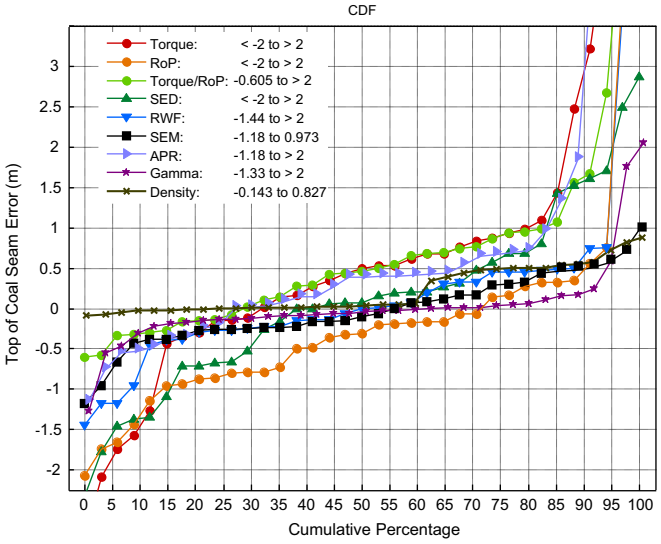

Fig. 12. Cumulative error distribution for various measures.

5.3. *MWD responses across coal seam boundary*

This section examines the behavior of several MWD measures as the rotary drills approach the coal band. Of special interest are the mechanical responses in the critical region, which refers to a ± 2 m buffer centered about the coal seam interface. This region encompasses both the overburden and coal seam. By design, the coal seam top boundary is aligned with the midpoint of the horizontal axis ($d=0$) to ensure the relatively hard (sandstone–siltstone layers) and relatively soft (carbonaceous–coal) material occupy the left and right half planes, respectively.

In Fig. 13, the MWD measures (RoP, SED, RWF and SEM) are shown from top to bottom. The left panels show the amount of variation in the MWD response as a function of the distance from the top-of-coal-seam interface. Each color strand represents one set of measurements down a blast hole.

For RoP and SED, as the coal boundary is approached from the left, the erratic criss-crossing pattern suggests a simple thresholding strategy will perform poorly and be highly susceptible to noise. Indeed, the level of coherence observed in the MWD signals provides confirmation for the statistics reported in Table 8 where for instance, the error standard deviations for SED and SEM detection are 1.14 m and 0.44 m, respectively.

The middle panels show the one standard deviation envelop about the mean response for each MWD measure. One constant feature is that both RWF and SEM exhibit lower variability compared to SED. Graphically, drawing a horizontal line about the mean at $d=0$ provides a good indication of the spatial uncertainty. Consider the line segment formed by the intersecting points of the horizontal line with the envelop. The span of this line segment (see black arrow) is an indication of how well the coal seam can be localized. When the segment is very long, there is large variability. This means, the coal seam boundary will often be detected too early or too late.

The right panels show the density estimates for each measure in the transition region. The diffused point clouds (the area enclosed by the dark blue contour bands) highlight the vulnerability of the RoP and SED measures with respect to noisy observations. For a graphical proof, one may draw a horizontal line along the bottom edge of the SEM image, then gradually move this line up toward zero (the SEM detection threshold), without hitting any points to the left of the coal seam boundary. Repeating this for SED, the contrary is true. Each point encountered actually results in a false positive.

The tight clustering of the SEM and RWF responses in Fig. 13 (right) demonstrates greater consistency and a higher margin for error relative to SED and RoP. Furthermore, the arrows that represent the 90% confidence interval is shortest for SEM and longest for RoP.

6. Discussion

This paper has shown that reliable coal seam detection can be achieved in a monitor-while-drilling context even without geophysical data. Using the rotation-to-thrust power ratio, the proposed SEM measure is able to detect the top of coal consistently with high specificity. Two avenues for implementing the detection logic were considered: one involves thresholding the SEM, the other uses an artificial neural network. Crucially, a neural network is not required to achieve near optimal coal seam detection performance. This finding is very encouraging, as the end-users need not be concerned with the complexity of training a neural network, or re-learning its parameters. Also, the thresholding policy in (10) is trivial to implement.

In terms of technology readiness, the authors are of the opinion that the hardware and software infrastructures that currently exist are already mature enough to support SEM integration. The main challenges actually pertain to the reliability of the MWD derived measure which the SEM has substantially dealt with. Today, MWD signals are routinely collected from sensors and monitored by drill operators in real-time. However, the level of analysis does vary from the simple to the sophisticated. The system and associated interface for sending commands to the actuators (drilling equipment) already exists on many integrated platforms. Typically, the MWD data is logged by an automated drill monitoring system and the analytic results (such as SEM graphics) are displayed while drilling takes place in the operator's cabin. To bridge the input and output paths, the computational unit needs only implement the SEM algorithm at the client's front-end. Neither this nor the decision-control feedback loop introduces a significant delay that impacts on real-time instrumentation. The SEM coal seam detection logic is envisaged as a plug-in module in an otherwise complete system. The middleware required to support data streaming and communication presumably already exists and thus allows MWD signals to be processed while drilling, and a “stop drilling” command to be issued using a software generated trigger.

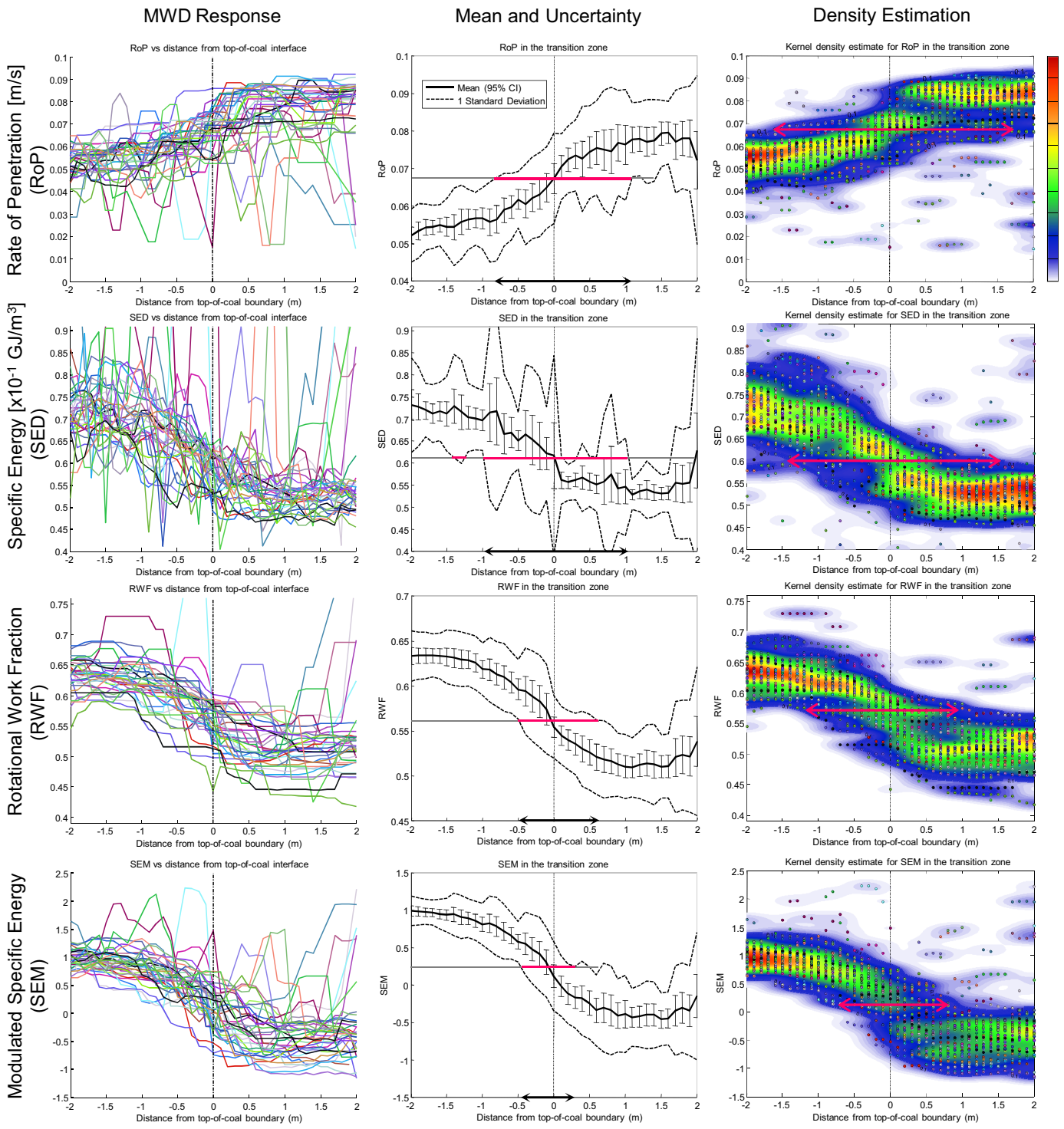

Fig. 13. Behavior of MWD measures (RoP, SED, RWF and SEM) in the critical region. (Left) MWD responses in the transition region as a function of the distance from the coal boundary. (Middle) 95% CI about the mean response and the 1 standard deviation envelop. Arrow roughly translates to 1σ uncertainty. (Right) Kernel density estimation of MWD response. Arrow indicates the spread at 2σ around the detection threshold. (For interpretation of the references to color in this figure, the reader is referred to the web version of this paper.)

One of the assumptions behind this work is that the drilling dynamics are invariant with depth. For this study, this is a reasonable assumption, since the rotary drill rigs are equipped with a PID controller which regulates drilling dynamics. In [27], a mechanism is described for compensating certain disturbances to maintain the torque at an operator configured set point. The embedded sensors can detect, for instance, mast vibration and changes in bit air pressure, and use the error signal to drive the control valve to modulate the pull-down pressure to provide a substantially constant torque. Whilst this may not cover all bases, it at least provides a steady platform for taking MWD measurements, and may explain the absence of linear variations in torque with depth. In spite of frictional energy loss and bit wear, such variations were not observed for depths of up to 40 m.

In relation to how the reported performance may translate to other drills in general, it is important to establish the operating

Table 9
Nominal operating conditions of rotary drills.

	Rotary speed (rpm)	Torque (kN m)	Penetration rate (m/s)	Weight on bit (kN)
Process Mean $\bar{\mu}$	142.5	6.713	0.0449	1045
Process S.D. $\bar{\sigma}$	9.642	0.622	0.0163	70.11
Max observed S.D.	32.52	1.926	0.0890	201.3

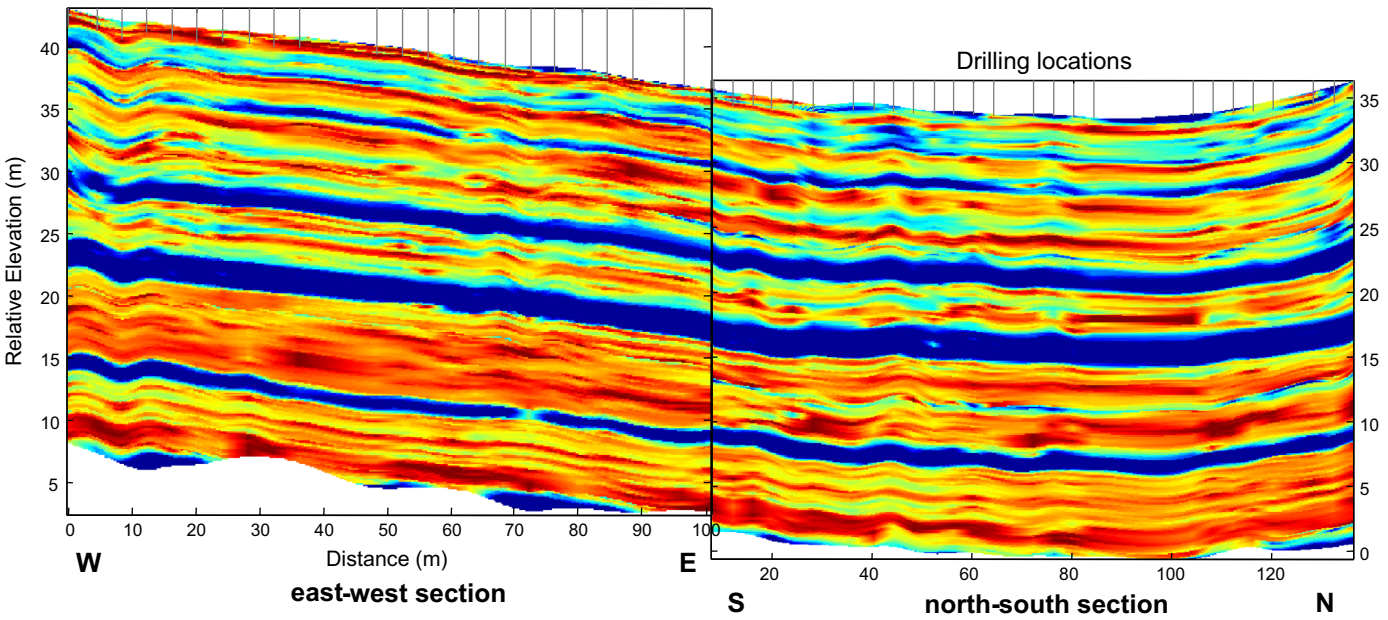

Fig. 14. SEM being tested in a different site using a different drill. The east–west and north–south cross-sections reveal multiple coal seams below the bench.

conditions encountered in this study. These nominal drill operating parameters are reported in Table 9. Based on results gathered from additional field trials conducted outside this study, the authors observed no deterioration in SEM performance when the MWD parameters (rotary speed, WoB, etc.) vary by up to 3 sigma (standard deviations). Even when the nominal conditions are not strictly satisfied, there is still scope for adjusting the sigmoid pivot value (c_0 in (6)) and SED gain (k_{SED} in (5)) to compensate for small level shifts in the signals to keep the SEM threshold invariant.

6.1. Final observations

Fig. 14 shows some additional SEM results obtained from a field trial. On this occasion, blast holes were drilled along two perpendicular rows. The 'L-shape' configuration allows two separate but related cross-sectional views to be joined together. The image clearly reveals multiple coal seams below the drilled bench. Significantly, this involved using a different drill at a different site, without any calibration of the default parameters. This illustrates the resilience of the SEM algorithm.

7. Conclusion

This paper proposed a coal-seam detection measure called SEM (modulated specific energy) which utilizes a hypothesized link between geomechanics and drill performance to detect the top of coal. Even though a direct relationship to the shear strength of rock strata had not been proven, the results demonstrated that accurate coal seam detection can be achieved using only MWD (monitor-while-drilling) data, without geophysical measurements such as bulk density. This is a significant step forward given the MWD constraints.

In rotary drilling, SEM can distinguish coal and non-coal rock layers with remarkable consistency by exploiting differences in the rotation-to-thrust power ratio. Its efficacy was demonstrated using mutual information, linear and nonlinear classifiers via a simple threshold strategy and artificial neural network. Importantly, the thresholding strategy may be used in place of the neural network without sacrificing detection performance.

Acknowledgment

This work has been supported by the Australian Centre for Field Robotics and the Rio Tinto Centre for Mine Automation. The authors would like to acknowledge Rio Tinto Technology & Innovation for providing the drill data used in the experiments. We extend our appreciation to our colleagues: Peter Hatherly, Cathy Zhou, Juan Nieto, James Underwood, Sildomar Monteiro, Nasir Ahsan, Arman Melkumyan, Ross Hennessy and HVO for their feedback, discussion and involvement in different aspects of the project. The reviewers are thanked for their comments and critique of this paper.

References

[1] Celada B, Galera J, Muñoz C, Tardáguila I. The use of specific drilling energy for rock mass characterisation and TBM driving during tunnel construction. In: ITA-AITES world tunnel congress, Budapest, Hungary; 2009.
[2] LaBelle D, Bares J, Nourbakhsh I. Material classification by drilling. In: International symposium on automation and robotics in construction and mining (ISARC), IAARC, Taipei; 2000. p. 91 TA3.

[3] Teale R. The concept of specific energy in rock drilling. Int J Rock Mech Min Sci Geomech Abstr. 1965;2(1):57–73.
[4] Scoble M, Peck J. A technique for ground characterization using automated production drill monitoring. Int J Surf Min Reclam Environ 1987;1(1):41–54.
[5] Scoble M, Peck J, Hendricks C. Correlation between rotary drill performance parameters and borehole geophysical logging. Min Sci Technol 1989;8(3):301–12.
[6] Sudheer Kumar D, Harish U, Sukumar G, Sreenath Reddy L. Microcontroller based radiometric density gauge (project). Technical report, Instruments and Systems Division, Electronics Corp. of India Ltd. (ECIL), Hyderabad; 2009. URL: ⟨http://www.scribd.com/doc/20052388/Documentation-of-Radiometry⟩.
[7] Haykin S. Neural networks: a comprehensive foundation. New Jersey: Prentice-Hall; 1999.
[8] Basheer I, Hajmeer M. Artificial neural networks: fundamentals, computing, design, and application. J Microbiol Methods 2000;43(1):3–31.
[9] Martin Gonzalez J. Application of pattern recognition techniques to monitoring-while-drilling on a rotary electric blasthole drill at an open-pit coal mine [Master's thesis]. Dept. Mining Engineering, Queen's University, Ontario, Canada; 2007.
[10] Özgen Karacan C. Elastic and shear moduli of coal measure rocks derived from basic well logs using fractal statistics and radial basis functions. Int J Rock Mech Min Sci 2009;46(8):1281–95.
[11] Hoek E, Marinos P, Benissi M. Applicability of the geological strength index (GSI) classification for very weak and sheared rock masses. The case of the Athens Schist Formation. Bull Eng Geol Environ 1998;57(2):151–60.
[12] Ulusay R, Yoleri MF. Shear strength characteristics of discontinuities in weak, stratified, clay-bearing coal measures encountered in Turkish surface coal mining. Bull Int Assoc Eng Geol 1993;48(1):109–17.
[13] Peng S, Patrick C, Khair A. Direct shear strength of Appalachian coal. Geotechn Test J (U S A) 1983;6(3):144–50.
[14] Chang C, Zoback MD, Khaksar A. Empirical relations between rock strength and physical properties in sedimentary rocks. J Pet Sci Eng 2006;51:223–37.
[15] Schöpfer MP, Abe S, Childs C, Walsh JJ. The impact of porosity and crack density on the elasticity, strength and friction of cohesive granular materials: insights from DEM modelling. Int J Rock Mech Min Sci 2009;46(2):250–61.
[16] Poulsen B, Adhikary D. A numerical study of the scale effect in coal strength. Int J Rock Mech Min Sci 2013;63:62–71.
[17] Gentzis T, Deisman N, Chalaturnyk RJ. Geomechanical properties and permeability of coals from the Foothills and Mountain regions of western Canada. Int J Coal Geol 2007;69(3):153–64.
[18] Segui J, Higgins M. Blast design using measurement while drilling parameters. Fragblast 2002;6(3–4):287–99.
[19] Zhou H, Hatherly P, Monteiro ST, Ramos F, Oppolzer F, Nettleton E, et al. Automatic rock recognition from drilling performance data. In: International conference on robotics and automation. St Paul, Minnesota: IEEE; 2012. p. 3407–12.
[20] Rasmussen CE, Williams C. Gaussian processes for machine learning. Cambridge, MA: MIT Press; 2006.
[21] Geoscience Australia. Coal fact sheet: Australian Mines Atlas. URL: ⟨http://www.australianminesatlas.gov.au/education/fact_sheets/coal.html⟩.
[22] Gray RM. Entropy and information theory. 2nd ed. New York: Springer. 2011 URL: ⟨ee.stanford.edu/~gray/it.html⟩.
[23] Rasmussen CE. Conjugate gradient optimization software. URL: ⟨http://sprinkler.googlecode.com/svn/trunk/regression/fmincg.m⟩.
[24] Hatherly P. Overview on the application of geophysics in coal mining. Int J Coal Geol 2013;114:74–84.
[25] Strange AD, Ralston JC, Chandran V. Near-surface interface detection for coal mining applications using bispectral features and GPR. Subsurf Sens Technol Appl 2005;6(2):125–49.
[26] Monteiro ST, Van De Ven J, Ramos F, Hatherly P. Learning 3D geological structure from drill-rig sensors for automated mining. In: International joint conference on artificial intelligence, vol. 3. AAAI Press; 2011. p. 2500–06.
[27] Edlund HE, Haines ML. Drill automation control system. US patent 5465798, Reedrill, Inc., Denison, Texas.